2020-03

Modeling the effect of storm-water flow on sewer system leakage

Baseka, Sifa Yohana

NM-AIST

https://doi.org/10.58694/20.500.12479/921

MODELING THE EFFECT OF STORM-WATER FLOW ON SEWER SYSTEM LEAKAGE

Sifa Yohana Baseka

A Dissertation Submitted in Partial Fulfilment of the Requirements for the Degree of Master's in Mathematical and Computer Science and Engineering of the Nelson Mandela African Institution of Science and Technology

Arusha, Tanzania

March, 2020

ABSTRACT

The storm-water overflow on manhole is numerically solved in this study. To produce a real representation of storm overflow, the Navier-Stokes equations were used. Turbulence flow was modelled using the standard k-epsilon turbulence model together with the volume of fluid method for phase surface tracking. The open-source fluid dynamics tool OpenFOAM 5.0 was used for solving the model and the visualization tool, paraview 5.4.0, was used for processing the solution data. The convergence test was performed at three different mesh sizes. The numerical solution was independent of mesh sizes. The risen storm-water column inside a manhole exerts a non-uniform pressure on the manhole cover. The non-uniform pressure distribution leads to different uplifting forces at manhole cover areas. However, the global uplifting force remains constant as long as the storm-water overflow is happening on the manhole. The overflow intensity is on manhole, and areas opposite to the outlet pipe give the highest intensity of the leaking storm-water. The rate of storm-water column rise inside a manhole is reduced by the use of manholes with larger width (or diameters) and pipes of larger diameters.

DECLARATION

I, Sifa Yohana Baseka do hereby declare that this dissertation is my own original work and that it has neither been submitted nor presented in any other institution for the degree award. All sources of Materials used in this dissertation have been fully acknowledged.

Sifa Yohana Baseka (Candidate)	Date
Professor Verdiana Grace Masanja**,** (Supervisor)	**Date**

COPYRIGHT

CERTIFICATION

The undersigned certify that has read and hereby recommend for acceptance by the Nelson Mandela African Institution of Science and Technology (NM-AIST) in Arusha, the dissertation titled: Modelling the Effect of Storm-water on Sewer System Leakage, in partial fulfilment of the requirements for the Master's degree in Mathematical and Computational Sciences and Engineering of the Nelson Mandela African Institution of Science and Technology.

Professor Verdiana Grace Masanja,
(Supervisor)

Date……

ACKNOWLEDGEMENT

Firstly, I want to thank God for giving me a special opportunity to join the Master's program at the Nelson Mandela African Institution of Science and Technology (NM-AIST).

Special thanks and credits to my sincere supervisor Prof. V. Grace Masanja, Professor of Computational Mathematics School of Computation and Communication Science and Engineering (CoCSE), (NM-AIST). I appreciate all her contributions of time, ideas and expert advice to make my Master's dissertation to be completed. I also humbly give thanks to Eng. Joseph D. Lwanyaga from Department of Mechanical Engineering, College of Engineering Design, Art and Technology, Makerere University Kampala for his support on the use of open-source CFD tool OpenFOAM, for numerically solving and simulations of fluid flow problems. His diligent efforts to ensure that other students become aware of how to use this tool will be unforgettable.

Great tribute to my sponsor, the African Development Bank (AfDB) for its financial support on this study. The scholarship was a vital component of the success of this work.

Great thanks to my parents, Yohana B. Gwibikiye & Debora N. Mlungisi for their support and encouragement and endless prayers. Without them, this work could have not been successfully accomplished. I would also like to thank my beloved brothers, Israel and Emmanuel, and-my beloved sisters Zera, Naomi, Amina and Devota for their best wishes on my studies. My lifetime at NM-AIST was a great moment due to friends and classmates that became part of my life. I am grateful for the time spent with University-mate and friends in social and academic activities.

DEDICATION

To you, Yohana B. Gwibikiye and Debora N. Mlungisi, my beloved parents I dedicate this dissertation.

TABLE OF CONTENTS

LIST OF TABLES

LIST OF FIGURES

LIST OF APPENDICES

LIST OF ABBREVIATIONS AND SYMBOLS

VOF	Volume Of Fluid
SPH	Smooth Particle Hydrodynamics
CFD	Computational Fluid Dynamics
OpenFOAM	Open Field Operation And Manipulation
NM-AIST	Nelson Mandela African Institution of Science and Technology
AfDB	African Development Bank

CHAPTER ONE

INTRODUCTION

1.1 Background of the problem

The problem of sewer leakage results in the spilling of wastewater to the environment, which is highly noted during rainfall. The leakage from the sewer system can occur in different ways like leakage from broken pipes, open channels' overflow and the overflow of manholes. The focus of this research is to model the wastewater overflow in manhole due to storm-water inflow into sewer systems during heavy rainfall and investigate the pressure head uplifting forces to the manhole cover.

People residences, commercial areas like markets, institutional areas and industrial areas, are the main producers of urban wastewater. Waste water leakage in cities and other towns, is a threat to human health as well as environmental sanitation. They are collected and transported through the existing urban sewer networks which are composed of detention ponds or tanks, sewer pipes, manholes, force mains, septic tanks, treatment plants, and waste disposal areas (Moeini & Afshar, 2017). Each component of the sewer network is crucial like the treatment plants which are responsible for changing the chemical behaviour of wastewater to reduce or eliminate the health or environment problems upon their discharge (Swamee & Sharma, 2013). These systems are complex, as they depend on geographical distribution with a hierarchical structure.

Sewer systems are designed to take household wastewater from toilets, bathrooms, showers, and kitchen sinks as well as wastewater from industrial and commercial buildings. The inflow of storm-water to the systems leads to overloading due to the combination of sewer flow and storm water. The overloading can be the cause of leakage through broken parts, as well as overflow in manholes and treatment plants (Chang,Wang & Chen, 2018). This study focused on the overflow phenomenon of wastewater on manholes due to the storm-water inflow to the systems during rainfall.

Manholes are essential elements found on these systems for various purposes like having access to the underground pipelines for regular maintenance, making the connection between pipes of different sizes, and where there is a need for the change of sewer line directions. They are also used where there is an elevation change between the pipes.

1.2. Statement of the problem

Many towns and cities in our country like Dar es Salaam and Arusha, sewer systems have not been improved to meet with the increasing population of residence buildings and industrialization (Pastore, 2015). Cities are still encountering spillage of sewage or wastewater on streets and homes massively during rainfall, which put human properties, environment sanitary and health of people at risk.

Various studies have been undertaken in the field of sewage systems for the main purpose of ensuring that collection, transportation, and deposition of wastewater are achieved to the required level such as those done by Beg, Carvalho and Lopes (2016) and Sánchez, Kaiser and Viedma (2016). These studies have focused on areas like the optimization of the sewer systems, improvements on the performance of treatment plants and the least cost design of detention tanks.

Despite efforts done in solving problems related to sewer systems, still, some challenges continue to exist such as leakage of wastewater from the system (Nawrot, Matz & Blazejewski, 2018). There is a little attention been paid to the understanding of overflow dynamics through manholes under the contribution of storm-water during rainfall. Therefore, it is the aim of this study to model the wastewater overflow on manholes due to storm-water inflow into sewer systems during heavy rainfall and investigate the pressure head uplifting forces to the manhole cover.

1.3. Rationale of the study

Different researches in addressing challenges on sewer systems have not focused on the leakage of the sewer system specifically on one of the elements, the manhole. This study is focusing on the modelling of overflow of waste water on manhole due to the inflow of storm-water and identify the uplifting forces exerted on the cover. The identified uplifting forces will help to determine the minimum weight of manhole cover required to prevent the leakage due to the vertical dynamics of the covers. The study can be extended to produce the minimum weight of manhole covers required for all manholes currently being used in the system.

1.4 Objectives

1.4.1 General objective

The general objective of this study is to develop and analyse a mathematical model for the sewer system leakage through manholes and investigate the manhole pressure head uplifting forces for controlling the leakage through manhole covers.

1.4.2 Specific objectives

The specific objectives of this study are;

(i) To model the overflow phenomena inside manholes due to the turbulent inflow of storm-water into the sewer systems during rainfall

(ii) To analyse the uplifting forces of the pressure head inside manholes from the mathematical model developed using CFD tools

(iii) To compare the inlet and outlet pipe diameter variations against manhole width (diameter) variations on the rate of storm-water column rise inside manholes.

1.5 Research questions

The research study was guided by the following questions:

(i) Which model is suitable for the overflow phenomenon inside manholes due to the inflow of storm-water into the sewer systems?

(ii) Which methods and tools can be used to analyse the uplifting forces from the model formulated?

(iii) Which variations between pipe diameter variations and manhole width (diameter) variations increase the rate of storm-water rise in manholes?

1.6 The significance of the study

This study will give a mathematical understanding of the phenomenon of how wastewater overflow is happening through manholes under storm-water contributions. This information can assist in the technical design of sewer systems that do not allow leakage through manholes. It will contribute to the design of sewer systems with maximum transportation of sewage to the treatment plants and thus rendering disposal to be safe. Also, the findings of the study will be beneficial to city authorities responsible for the management of sewage disposal, sewer network designers and researchers in waste water field.

1.7 Delineation of the study

The main focus of this project was the modelling of an overflow phenomenon of waste water in sewer system. The study used the fluid dynamics properties to model the flow of storm water inside the system. The calculation and simulation was done by the CFD open source tool, OpenFOAM 5.0. The simulation was limited only to a single rectangular manhole with width 1meter and height 1.5 m. The simulation can be done for any type of manhole with any dimension. Some assumptions were used on the model equations for the proper simulation of the real situation.

1.8. Conceptual framework

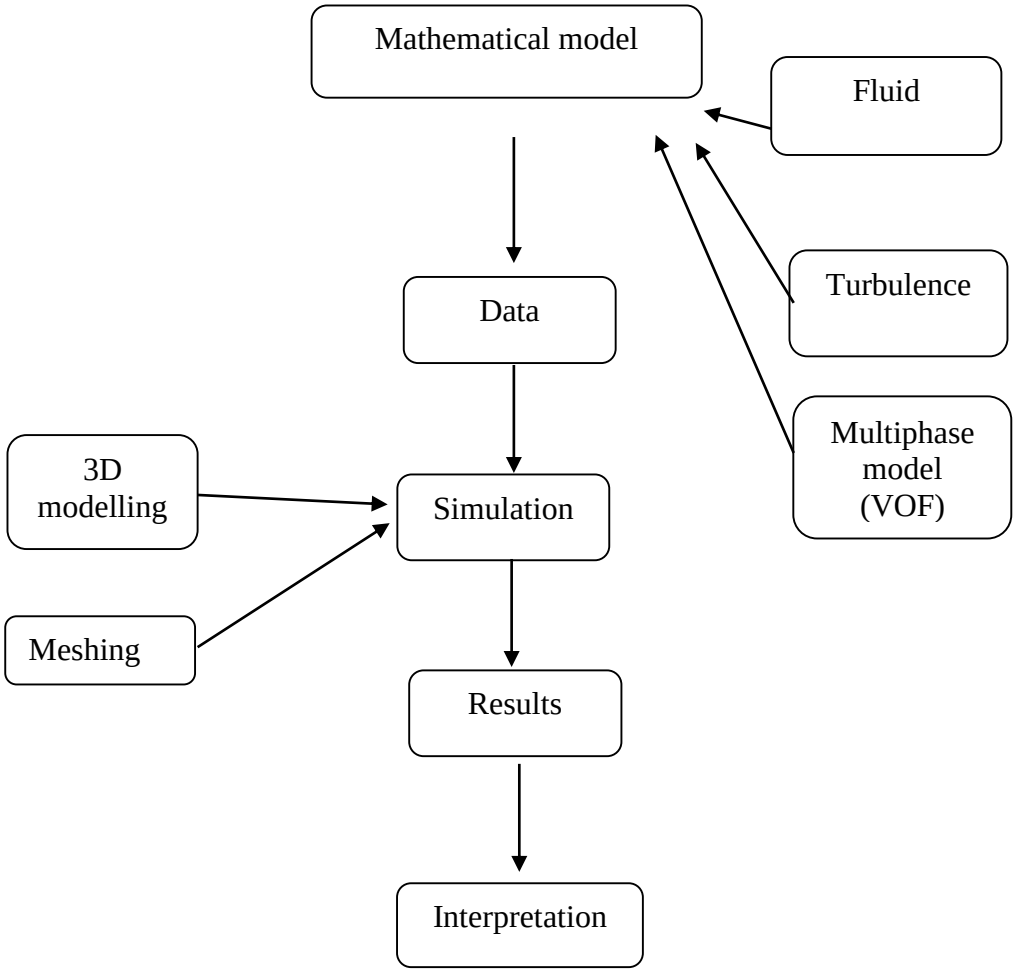

Figure 1: Conceptual framework

CHAPTER TWO

LITERATURE REVIEW

2.1 Introduction

This chapter is concerned with a literature review about sewer systems in urban areas. The review from previous work is categorized into three areas which are sewer network optimization, wastewater treatment, and sewer hydraulics within pipes and manholes due to different inlets like drainage and sewage from the network.

2.2 Sewer network optimization

The sewer networks are used to collect, transport, treat and deposit the wastewater that comes from domestic, industrial, institutional and business places. Usually, the installation cost of the sewer network is large and upon finding the possible minimum installation cost, Villiers, Rooyen and Middendorf (2019), suggested that the optimal diameters and pipe slopes should be determined. The cost function for the installation cost is given in equation (1),

$$C = \sum_{i=0}^{N} L_i K_i \left(d_i, E^{ave} \right) + \sum_{j=0}^{M} K_j h_j \tag{1}$$

where C is the cost function, L_i is the i^{th} pipe length, K_i is the unit cost function of the i^{th} pipe, K_j is the unit cost function of the j^{th} manhole, d_i is the diameter of the i^{th} pipe, E^{ave} is the average cover depth, h_j the height of the jth manhole, N is the number of pipes in the sewer network and M is the number of manholes in the sewer network. The right-hand side terms of the equation correspond to the pipes and manholes installation costs respectively. For the minimal optimization of the sewer network installation cost, it was recommended that the optimal pipe slopes, diameters, and manhole sizes should be determined. However, the study didn't focus on the leakage challenges in these sewer networks.

Duque and Saldarriage (2017), performed a study concerning the design of pipe series in sewer systems. By using the shortest-path problem, the study proposed the use of graph modelling to determine the minimum cost for the design of the series of pipes in sewer systems. The results show that lower values of pipes elevations (slopes) and larger values of the pipe's diameter help the minimum cost design of the pipe series while maintaining the sewer flow. The study's

methodology didn't use the unsimplified hydraulic constraints in the production of the optimal solution, rather it considered the computational time by using limited resources.

2.3 Waste water treatment

The treatment of sewer water in Waste Water Treatment Plants is there for modification of wastewater properties for the safe environment disposal or reuse purposes. A biological process, among the processes in treatment, incorporates the oxidation process for the removal of dissolved contaminants in activated sludge plants. Computational Fluids Dynamics was used by Sánchez *et al*. (2016), in the simulation of the activated sludge plant in two processes, aerated simulation, and un-aerated simulation. It was established that there is an improvement in the plant performance with aeration since it results in the reduction of stagnant volume and residence time. Also, there is a notable change in the velocity field and free surface level. Dealing with solving treatment plants challenges, the study didn't focus on the leakage related challenges on the sewer systems.

Meister and Rauch (2016), described the necessity of wastewater treatment through the model based on smooth particle hydrodynamics (SPH) in the biological stage. By using the model, an investigation was done on the stirrer, aeration mixing and the concentrations of the biokinetic compounds. The method resulted in a high resolution of biokinetic concentrations solution within a treatment plant. In this method, they used the continuity equation, equation 2 to control the rate of change of the densities for fluid particles. And the particles' velocities are determined from the momentum differential equation, equation 3,

$$\frac{\partial \rho_i}{\partial t} = \rho_i \sum_j v_{ij} \nabla_i w_{ij} m_j / \rho_j \tag{2}$$

$$\frac{\partial v_i}{\partial t} = -m_i \sum_j \left(\rho_i^{-2} + \rho_j^{-2}\right)\left(\rho_i p_j + \rho_j p_i\right)\left(\rho_i + \rho_j\right)^{-1} \nabla_i w_{ij} + \frac{F^v}{m_i} \tag{3}$$

where the right-hand side of equation 3 corresponds, respectively, to the pressure gradient term, the viscous force term, and the gravitational term. v is the particle velocity, m is the particle mass, w the particle weight, ρ the particle density, F^v are the viscous forces and g the gravitational acceleration. The study suggested that CFD was an appropriate tool for wastewater treatment simulations since both the effect of multiphase flow and biokinetic models can be incorporated.

2.4 Waste water hydraulics

Based on the role, gully structure plays on linked manholes, Beg, Carvalho and Leandro (2016), analysed the flow behaviour of the gully-manhole drainage structure in sewer systems, Fig. 2. To compute and simulate results, the study made use of InterFoam, an OpenFOAM solver for the incompressible and immiscible two-phase flow that deals with Reynolds's averaged equations, i.e., equations 4 and 5,

$$\nabla.\vec{u} = 0 \tag{4}$$

$$\frac{\partial \rho \vec{u}}{\partial t} + \nabla.(\rho \vec{u}\vec{u}) = -\nabla.\tau + g.x\nabla\rho + f_\sigma \tag{5}$$

where $\vec{u}$ is the velocity, p is static pressure, x is distance moved against the gravitational field, τ is the stress tensor, g is gravitational acceleration and f_σ is the force due to surface tension. The study established that in the gully manhole structure, intercepted precipitation flow on the ground surface to the gully decreases with increasing surcharge height in manholes. Alongside this behaviour, it was observed shear stress values to be higher at the bottom of the gully than on the manhole floor. The shear stress information between gully and manholes shows that there is a possibility of transportation of large solid particles to the gully as well as sedimentation of these particles at the bottom of the manhole. Also, it was established that the flow pattern of the sewage is affected by surcharge height.

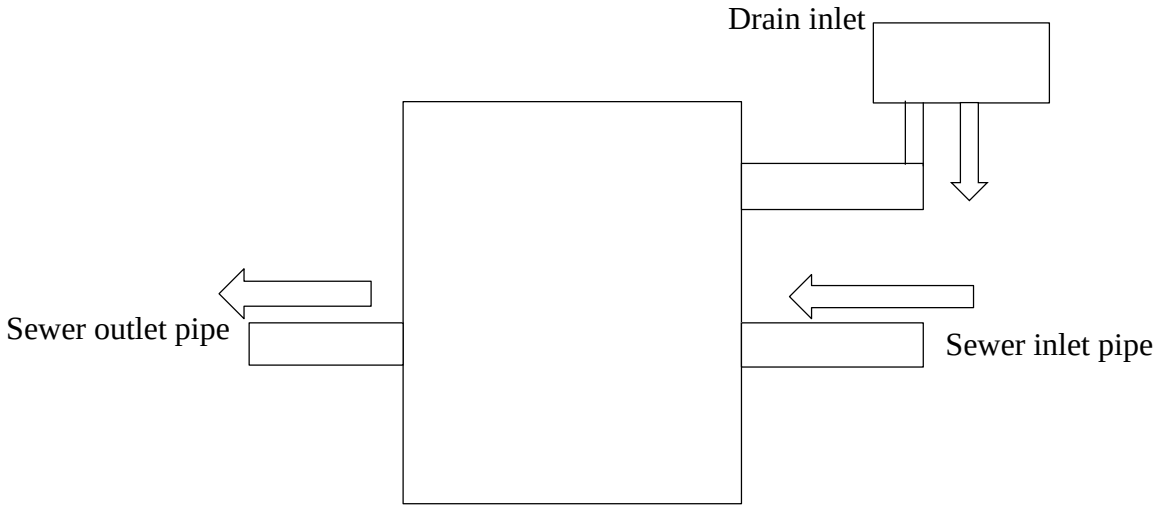

Figure 2: Gully-manhole

Beg, Carvalho and Lopez (2016), conducted a numerical study of the flow structure of wastewater inside a manhole for the purpose of understanding the sediment and suspended solid transport in the sewer systems to guide further studies. They observed that different flow

patterns of the flow inside manholes are brought about by different velocities at the inlet pipe. Also, they observed that different pressure levels due to the risen sewer column in the manhole, create different pressure gradients at the manhole flow which might be the source for uplifting forces to the suspended materials within the flow. However, this study did not consider the overflow of the wastewater that happens in manholes especially during rainfall.

Jo, Kim, Jung, Yoon and Sei (2018), prepared a physical model for investigating the head loss coefficient in a four-way junction manhole at its overflowing state due to different inlet flow rates at a 1:10 ratio. It was established that the head loss coefficient of the manhole at its overflowing state, increased in value from circular middle manholes to the right-angled junction manholes. The calculated head loss coefficient from varying inlet flows at a 1:10 ratio, was used to propose a head loss coefficient equation that can be used in the simulation of flow features of pipes and surface flow.

Head loss coefficients in manholes are factors that can contribute to the damage of the unit on flooding (Manholes, 2018). Higher values of these coefficients indicate the complicated passage of the flow from inlet pipes to the inside of manholes while manholes with low values of head loss coefficient have a smooth passage of wastewater. The study used numerical simulations to find a design for a four-way manhole that reduces the head loss coefficient. It was found that half rectangular benching designs should be used in circular four-way manholes as they reduce head loss coefficient than four-way square manholes. For full rectangular benching designs, they established that these should be used in four ways square manholes as they reduce head loss coefficient than circular manholes.

Nazmul, Rita and Jorge (2018), included gully element, and performed the numerical study to investigate the effect of manhole head loss coefficient and gully flow on different manhole surcharges and their effect on the general flow. They established that at different surcharge levels, there are significant effects on the gully-manhole flow. With gully flow, different surcharge levels change shear stresses within the manhole. For a higher surcharge, authors proposed that sedimentation is likely to happen at the bottom of the manhole.

During land vibrations like on earthquake, there is a significant loss in saturated soil strength which leads to soil liquefaction (Zhang & Chian, 2019). In determining the component forces acting on the interface between the manhole and surrounded soil, Zhang *et al.* (2019), contend that the interface friction forces are crucial regardless of their small magnitude. These friction

forces represent the proper position of residual resistance to the manhole uplift relative to other forces like the manhole weight. It was found that the increase of force per unit volume of soil from flowing water and the decrease in shear stress contribute much to putting the manhole stability.

Wang, Vascon, Vasconcelos and Jose (2019), investigated the physics behind vibration of the manhole cover during storm-water filling up into the sewer systems. The author considered this to be a nonlinear spring-mass system, whose model gave a lot of information on the mechanism of manhole cover vibrations. The study revealed that the air pressurization from air pockets in the water column inside the manhole and the rising water level inside the manhole have the ability to create the displacement of the manhole cover. It concluded that air pressurization and the rising water level are the two flow conditions that are associated with the displacement of the manhole cover. However, the study didn't use computational fluid dynamics in modelling the phenomenon; and didn't elaborate the forces of the filling up storm-water in manholes that keep the cover into vibrations.

All of the literature reviewed is concerned with solving different challenges associated with sewer systems. In working with leakage challenge of the sewer systems through manholes, neither of the studies determined the magnitude of the uplifting forces of the storm-water column inside the manhole. Therefore, this study investigated the overflow phenomenon of wastewater through manholes due to storm-water inflow and determined the uplifting forces of the storm-water column on hitting of the cover.

CHAPTER THREE

MATERIALS AND METHODS

3.1 Data collection

The data used for manhole were secondary data from the manhole multi-link experiment from Coimbra University laboratory, Portugal (Beg *et al*. 2016).

3.2 Methodology and model formulation

3.2.1 Model formulation

The first objective was to apply physical fluid properties to formulate a model associated with sewage overflow phenomenon on the manhole, due to storm-water inflow into sewer systems.

(i) Model assumptions

(a) Incompressible flow

Water flows are incompressible flow except for high speed moving gas (Xue & Barton, 2015). The volume of every portion of the moving water remains unchanged over the course of the time flow. Therefore, the flow of storm-water is an incompressible flow, its rate of change of density being equal to zero, equation 6.

$$\frac{\partial \rho}{\partial t} = 0 \tag{6}$$

(b) Newtonian flow

A Newtonian fluid is a fluid in which the viscous stresses from its flow are linearly proportional to the velocity gradient, equation 7, where x and y are indices for direction representation and τ_{xy} is shear stress acting along the x direction perpendicular to y direction. Water is a Newtonian fluid, once inflow, the shear stresses are linearly dependent to their velocity gradients (Khare, 2015).

$$\tau_{xy} = \mu\left(\frac{\partial u}{\partial y} + \frac{\partial v}{\partial x}\right) \tag{7}$$

(c) Turbulent and transient flow

Due to the random and rapid flow of storm-water over time that happens in full pipes, the flow is a turbulent one. Its velocity is expressed as the sum of two components, the fluctuating part v', and the averaged part $\bar{v}$. The flow variables like velocity, pressure and turbulent kinetic energy change with time. The flow is therefore a transient flow with variables' values changing with time.

(d) Isothermal flow

The storm-water flow in the sewer system is an isothermal flow, making heat transfer at constant temperatures. There are no significant temperature variations in the fluid being flowing (Factor, Pressure & Menon, 2015). There is an exchange of thermal energy between the flow system in the pipe and the surrounding environment which makes the temperature to remain constant within the flow.

(ii) Governing equations

Governing equations providing the basis for modelling fluid flow in this study are derived from conservation laws of mass, linear momentum, and energy after taking into consideration some appropriate assumptions (Ramakrishna, 2011). These equations express the conservation laws that must be satisfied for each control volume of the computational domain. The mass conservation law is expressed by the continuity equation; it ensures that the net inward mass flux is equal to the rate of change of mass in the computational domain. The linear momentum conservation law is expressed by the equations of motion also known as Navier-Stokes equations by which for each control volume, the sum of forces acting is regarded to be equal to the rate of change of momentum. The conservation of energy is expressed by the energy equation, it ensures the conservation of energy distribution on the flow.

(a) Continuity equation

Conservation of mass leads to the continuity equation, equation 8.

$$\frac{\partial \rho}{\partial t} + \nabla.(\rho \vec{u}) = 0 \tag{8}$$

With ρ the fluid density and $\vec{u}$ is the velocity vector whose components in rectangular cartesian coordinates are u, v and w in the x, y and z directions, respectively. The first term in equation 8 is the instantaneous change of density with time in the control volume while the

second term represents the rate of mass flux passing out of the control surface per unit volume. For incompressible flow, the continuity equation becomes equation 9, indicating a divergence-free velocity.

$$\nabla.\vec{u} = 0 \tag{9}$$

(b) Equations of motions

Conservation of linear momentum leads to the equations of motion, Eq. (10)

$$\frac{\partial}{\partial t}(\rho\vec{u}) + \nabla.(\rho\vec{u}\vec{u}) = -\nabla p + \nabla.\tau + \rho F \tag{10}$$

The body force F is force per unit mass and p is the pressure. τ in equation of motion is the viscous stress tensor. Equations of motion is the generalization of Newton's second law of motion for the conservation of linear momentum (Salih, 2011). The left-hand side of equation 10 represents the rate of change of momentum as the sum of two terms, the rate of increase of momentum per unit volume in the control volume (the first term) and the rate of momentum per unit volume lost by the bulk transport of fluid through the control surface. The right-hand side represents the net force that is exerted on the control volume which is the sum of body forces and surface forces. Body forces are exerted on the entire mass of the control volume while surface forces are acting on the faces of the control volume by the normal and shear stresses.

With constant properties, the equations of motion for incompressible flow are reduced to Navier-Stokes equations. By Reynolds decomposition approach on dependent variables of Navier-Stokes equations, the turbulence within the flow can be modelled. For an incompressible and turbulent flow under constant properties, the equations of motions equation 10 becomes Reynolds-Navier-Stokes equations, equation 11.

$$\frac{\partial\vec{u}}{\partial t} + \vec{u}.(\nabla\vec{u}) = -\frac{1}{\rho}\nabla p + \frac{\mu}{\rho}\nabla.\tau + g \tag{11}$$

With mean velocity vector $\vec{u}$, the gravitation g acting on the flow and p is the mean kinematic pressure. The term containing gravitational acceleration represents the weight per unit volume as the body force acting on the moving fluid. The components of the mean shear stress tensor τ_{ij}, for i, j taking values 1, 2, 3, are given by equation 12 with μ being the dynamic viscosity. The second term of the shear stress tensor represents the stress due to turbulent motion, the Reynolds stress term. It contains unknowns, the fluctuating velocity

components u_i' that are further modelled by using the Boussinesq hypothesis, where Reynolds stress is proportional to the mean velocity gradient, equation 13.

$$\tau = \tau_{ij} = \mu\left(\frac{\partial u_i}{\partial x_j} + \frac{\partial u_j}{\partial x_i}\right) - \rho\overline{u_i'u_j'} \tag{12}$$

$$-\rho\overline{u_i'u_j'} = \mu_t\left(\frac{\partial u_i}{\partial x_j} + \frac{\partial u_j}{\partial x_i}\right) - \rho\frac{2}{3}k\delta_{ij} \tag{13}$$

With ρ the fluid density, $\delta_{ij} = \begin{cases} 0 \ for\, i \neq j \\ 1 \ for\, i = j \end{cases}$ -is the Kronecker delta. The turbulent viscosity μ_t is given by equation 14. It depends on the kinetic energy k and its dissipation rate $\in$. C_μ, is the turbulent model constant equal to 0.09.

$$\mu_t = C_\mu \rho \frac{k^2}{\in}, \tag{14}$$

(c) Energy equation

For an incompressible fluid flow, the equation for conservation of energy is given by equation 15 where T is the absolute temperature, ϕ the dissipation function representing the work done against the viscous forces, c_p the specific heat capacity at constant pressure and ρ the fluid density (Sert, 2012).

$$\rho c_p\left(\frac{\partial T}{\partial t} + (u.\nabla)T\right) = k\nabla^2 T + \phi \tag{15}$$

For an isothermal flow, the temperature is constant therefore the velocity field in incompressible flow is independent of heat transfer and thermal effect (Factor *et al*., 2015). Velocity and pressure distribution may thus be solved without regard of the energy equation. Hence the energy equation is separated from the remaining conservation equations, the continuity and linear momentum equations (Khare, 2015).

(iii) Turbulence model

Reynolds's averaged Navier-Stokes Equation contains more unknowns than equations due to Reynolds stresses (Uddin & Karim, 2017). The k-epsilon ($k-\in$) is a two-equation model

making a closure to Reynolds averaged Navier-Stokes Equations for modelling turbulence stresses. It contains two transport equations, for turbulent kinetic energy k and for the rate of dissipation of turbulent kinetic energy $\in$. The turbulence kinetic energy k determines the kinetic energy in turbulence while the turbulence dissipation $\in$ determines the rate of dissipation of the turbulence kinetic energy. The $k-\in$ values are obtained by solving the two transport equations equation 16 and equation 17 which are used to find values for the turbulent kinematic viscosity μ_t in equation 14.

The turbulence kinetic energy transport equation is expressed as equation 16

$$\frac{\partial k}{\partial t}+u(\nabla k)=P^{(k)}-\in+\nabla.\left(\frac{\nu_t}{\sigma_k}\nabla k\right)+\nu\nabla.(\nabla k) \tag{16}$$

Dissipation rate of turbulent kinetic energy

$$\frac{\partial \in}{\partial t}+u(\nabla \in)=-C_{\in 1}\frac{\in}{k}P^{(k)}-C_{\in 2}\frac{\in^2}{k}+\nabla.\left(\frac{\nu_t}{\sigma_\in}\nabla \in\right)+\nu\nabla.(\nabla \in) \tag{17}$$

$P^{(k)}$ is the production rate of turbulent kinetic energy per unit mass and $C_{\in 1}, C_{\in 2}$ $\sigma_k, \sigma_\in$ are model constants.

In solving the model equations 20 to 23, the initial value for the turbulence kinetic energy and dissipation rate are estimated from relationships, equation 18 and equation 19,

$$k=\frac{3}{2}(uI)^2 \tag{18}$$

$$\in=C_\mu^{\frac{3}{4}}\frac{k^{\frac{3}{2}}}{l} \tag{19}$$

Where, C_μ is the turbulent model constant, k is the turbulent kinetic energy, $\in$ the dissipation rate and l is the turbulent length scale.

3.2.2 Model equations

The model of storm-water flow in the manhole is comprised of a set of partial differential equations, equation 20 to equation 23, consisting the Reynolds averaged-Navier-Stokes Equations, the transport equations for turbulent kinetic energy k, and the dissipation rate $\in$. The model equations will be solved together with boundary conditions described latter on page 17.

$$\nabla.\vec{u}=0 \tag{20}$$

$$\frac{\partial \vec{u}}{\partial t}+\vec{u}.(\nabla\vec{u})=-\nabla p+\nabla.\tau+g \tag{21}$$

$$\frac{\partial k}{\partial t} + \vec{u}(\nabla k) = P^{(k)} - \in + \nabla.\left(\frac{\nu_t}{\sigma_k}\nabla k\right) + \nu\nabla.(\nabla k) \tag{22}$$

$$\frac{\partial \in}{\partial t} + \vec{u}(\nabla \in) = -C_{\in 1}\frac{\in}{k}P^{(k)} - C_{\in 2}\frac{\in^2}{k} + \nabla.\left(\frac{\nu_t}{\sigma_\in}\nabla \in\right) + \nu\nabla.(\nabla \in) \tag{23}$$

This model needs to be numerically solved to determine the variable fields for mean velocity $\vec{u}$, pressure p, turbulent kinetic energy k, and the kinetic dissipation rate $\in$.

3.2.3 Computational domain

The geometry for the computational domain simulating storm-water overflow is the manhole illustrated in Fig. 3. The computational domain was designed using a free source 3D modelling software, FreeCad 0.18. The manhole (the large rectangular container) has two circular pipes joined to it, the inlet pipe and the outlet pipe. The inlet pipe is the part of the pipe that carries the entering storm-water to the manhole while the outlet pipe is the pipe that carries the flowing sewage which is coming out of the manhole to other parts of the sewer systems. The cover is placed at the top of the manhole. Here is where the overflow occurs during the exceeding of the system capacity.

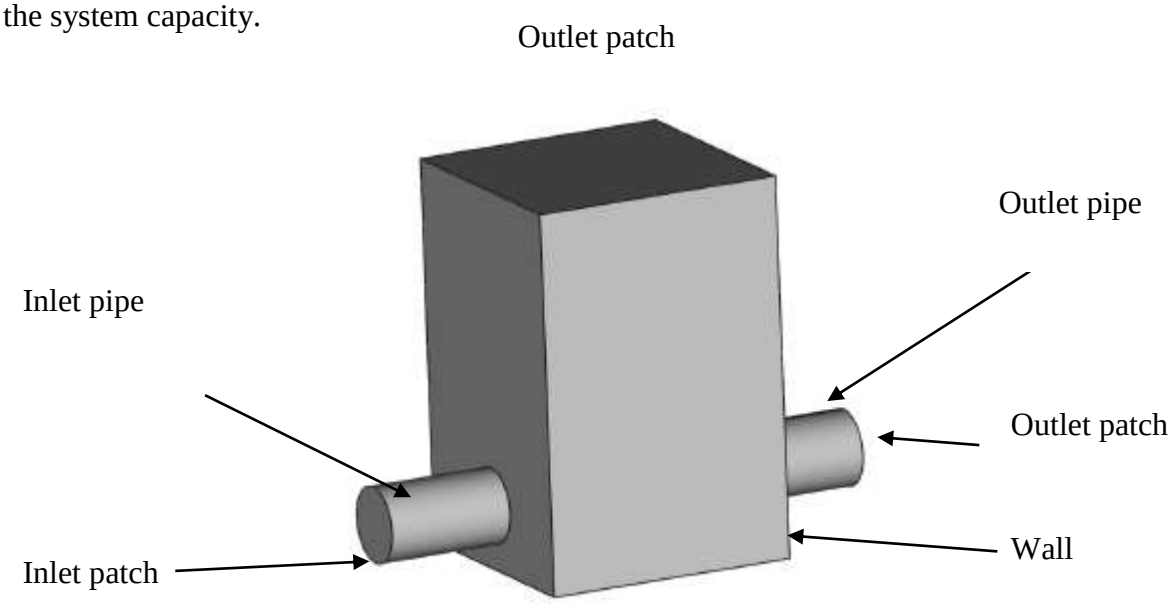

Figure 3: Manhole, the computational domain

The boundaries extracted from the geometry are inlet boundary, outlet boundary, and wall boundary. There are two outlet boundaries, the outlet boundary at the outlet pipe and outlet boundary at the top of the manhole. The inlet boundary is located at the patch of the inlet pipe whereas the outlet boundary is located at the patch of the outlet boundary. The outlet boundary

located at the top of the manhole is where the overflow of the sewer occurs due to the rising column inside the manhole. The wall boundary includes all stationary walls remaining from the geometry setup.

The mesh of the geometry was done by using block Mesh and snappyhexMesh utilities in OpenFOAM 5.0. The geometry STL files for the OpenFOAM 5.0 were prepared by the free 3D software FreeCad 0.18. To account for the vicious velocity gradient property at the walls, boundary layers were added to the stationary walls. The mesh for the geometry setup is given in Fig. 4.

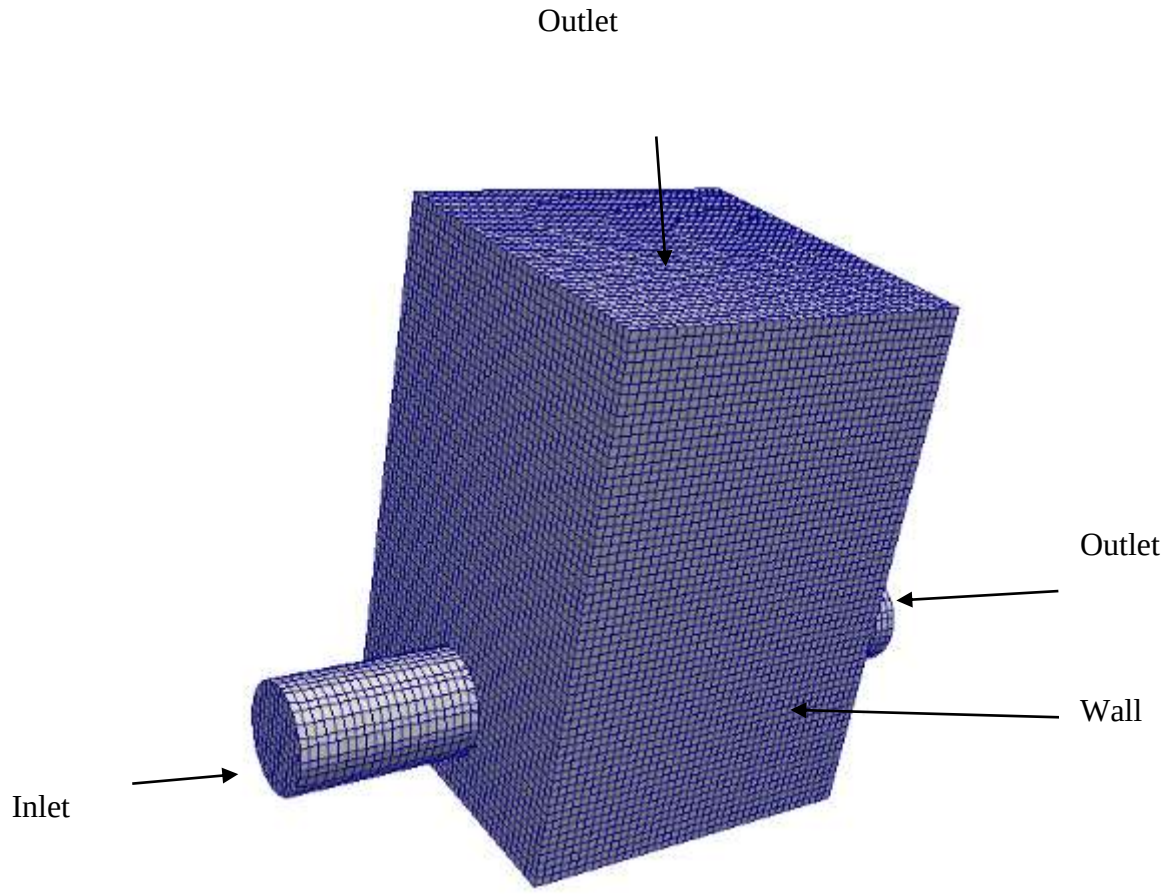

Figure 4: Mesh for the manhole

The whole of the computational domain consists of 243 000 cells. The summary for the mesh quality parameters, skewness, aspect ratio, non-orthogonality for high efficient simulations is given in Table 1.

Table 1: Maximum value for mesh quality parameters

Mesh parameter	Max skewness	Max aspect ratio	Non-orthogonality
value	3.08 378	7.81 836	72.9 549

3.2.4 Boundary conditions

From Fig. 4, there are three boundaries: inlet, outlet, and wall. The boundary condition at the inlet is a fixed value boundary condition. It is a Dirichlet boundary condition in OpenFOAM that allows the assignment of model variables' initial values to the inlet patch (Bayon, Valero & Garcia, 2016). Initial conditions for turbulent kinetic energy k, dissipation rate $\in$, velocity v are assigned using this boundary condition. The initial value for turbulent viscosity at the inlet patch is estimated using equation 14. The "calculated" boundary condition is used for this purpose, as it assigns the field value derived from other field values. The initial pressure field within the computational domain is defined by total pressure boundary condition which contains an entry p_0 for initializing the internal total pressure. This boundary condition provides total pressure condition, equation 24, for incompressible fluid flow, where p denotes static pressure, p_0 the total pressure and the last term is the dynamic pressure due to kinetic energy of the moving fluid (Ravelli, Barigozzi & Pasqua, 2014).

$$p = p_0 - \frac{1}{2}\rho u^2 \tag{24}$$

InletOutlet is the boundary condition in OpenFOAM which is used on outlet patches for k and $\in$. This is the zero gradient boundary condition that applies to the quantity field when the field is out of the domain. And it is a fixed value boundary condition as the field is flowing in the reverse direction. Since the quantity field at the outlet patch is unspecified, zero gradient boundary condition sets the gradient of quantity field to zero, so that it can be extrapolated from the nearest cells. InletOutlet boundary condition restricts the unwanted backflow of the quantity field though the value defined at the inletValue entry. For the velocity field at the outlet patch, pressureInletOutletVelocity is the boundary condition in OpenFOAM which is used due to the initial internal pressure specification.

The velocity field at a fluid-solid boundary is equal to the velocity field of the solid boundary (Moukalled, Mangani & Darwish, 2016). Therefore, at the walls, noSlip is the boundary condition in OpenFOAM used to account for the zero velocity of the viscous fluid.

3.2.5 Solver

InterFoam, a multiphase solver in OpenFOAM 5.0 was used for simulation of the storm-water overflow of the manhole. The solver solves the continuity and Naiver-Stokes equations for two incompressible, isothermal, immiscible, transient and turbulent fluids. The material properties such as the density, viscosity, and specific heat capacity are constant in the region filled by one of the two fluids except at the interphase (Rocco, Coppola & Luca, 2010). To capture the interphase between the two phases, interFoam employs the volume of fluid (VOF) method, a numerical technique for tracking and locating an interface between phases (Date, 2017). The model uses the volume fraction α to denote the individual phases. The volume fraction $\alpha = 1$ of the computational cell is completely filled with water and for $\alpha = 0$ if the cell is completely filled with air. The liquid-gas interface arises within mesh cells where α takes on values between 0 and 1. In order to know where the interphase is, the additional equation 25 for α is solved

$$\frac{\partial \alpha}{\partial t} + \nabla.(\alpha \vec{u}) = 0 \tag{25}$$

with $\vec{u}$ the mean velocity and α the volume fraction within a cell.

CHAPTER FOUR

RESULTS AND DISCUSSION

4.1 Introduction

The initial values for the turbulent kinetic energy, turbulent dissipation rate, pressure, and velocity were determined before solving the model. The radius of the inlet and outlet pipe of the computational domain is 0.15 m, making the hydraulic diameter of 0.3 m which was required in the calculation for various Reynolds numbers. After incorporating the initial and boundary conditions, the model results for the manhole overflow are given in Fig. 5.

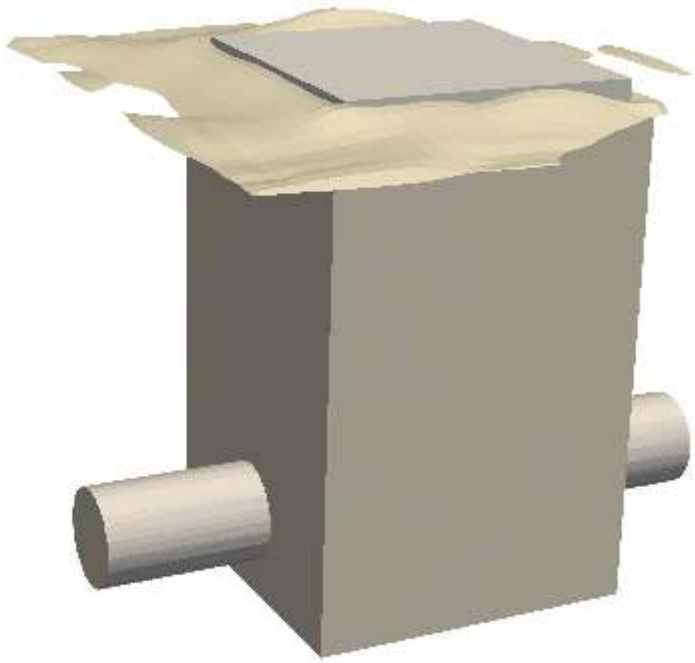

Figure 5: An overflowed manhole

4.2 Convergence test

Before simulations were done, the meshing test was done at three different meshes to ensure the independence of the model results on the discretization. The first mesh contained 243 000 cells, the second mesh had 415 000 cells and the last mesh had 600 000 cells. In order to converge, the model must give nearly the same results at different levels of mesh refinement. The pressure residual profile for the different meshes is shown in Fig. 6. The first mesh residual

is represented by the blue curve, the second mesh residual is represented by the yellow curve and the third mesh residual is represented by the green curve.

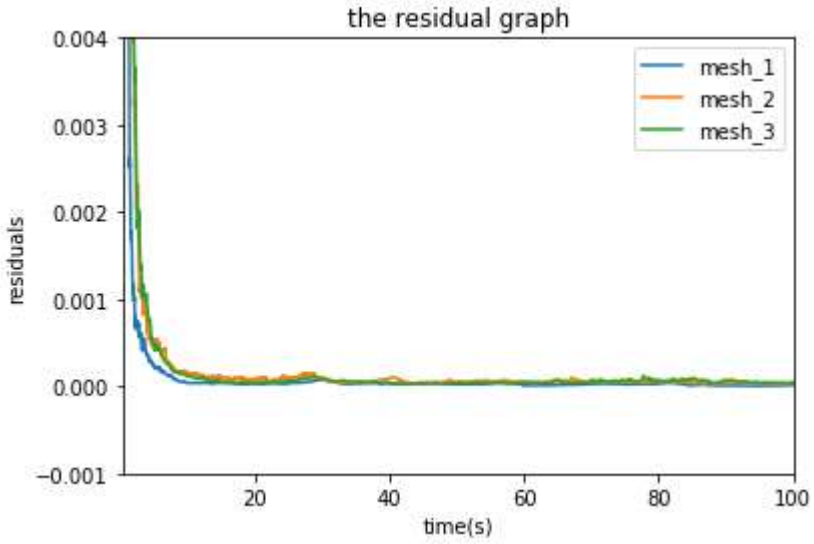

Figure 6: The velocity residual for different meshes.

From the graph, it can be seen that as the residuals decrease with increasing time, curves of all the three meshes are converging to the same result, until they attain a constant value. At $t \to 0$, the solution is not convergent yet, residuals take larger values. It can be observed in Fig. 6 that curves of the three different meshes are nearly coincident after attaining a steady solution, thus the difference between attained results by the three mesh sizes is negligible. Normally a finer mesh gives much better resolution on model results but it takes a quite a lot of computational time. Since in this case, the difference in results obtained by using the mesh of 243 000 cells and that of 600 000 cells is negligible, in order to reduce the computational time, the first mesh was chosen to do the computations and simulations for the storm-water overflow in the manhole.

The three mesh were further used to compare results of the magnitude of the velocity at the centre of the outlet pipe, 0.2 m from the manhole. The graph of the magnitude of velocity against the three meshes is almost a horizontal line, whose gradient is almost zero Fig. 7. This indicates that the rate of change of velocity values per change on the number of geometry cells is zero. This implies that the model computational is independent of the geometry of meshes.

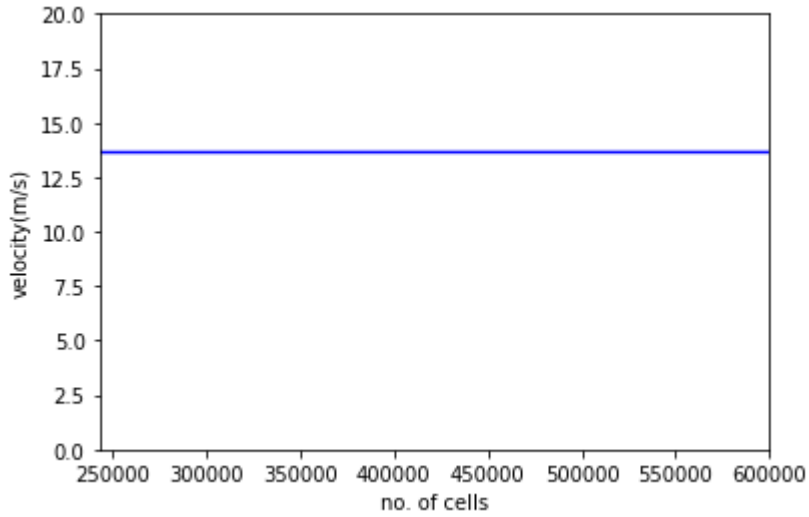

Figure 7: The velocity graph against mesh size

4.3 Experimental comparison

The numerical simulation for the sewer flow inside the manhole was compared with experimental results from two connected manholes setup at the University of Coimbra (Beg *et al*. 2016). The setup consists of two connected manholes each with a diameter of 1 m, and the inlet and outlet pipes each with 0.3 m diameter Fig. 8. The setup was used to measure pressure values at various points by using pressure sensors and measuring the height of the risen water column inside a manhole at different inflow rates of the water. After reaching a steady-state flow, the pressure values and water column heights inside the manhole were recorded.

Figure 8: Manhole experiment at Coimbra laboratory

To produce a similar representation of the model to the real situation, the numerical manhole simulation of this study is compared with experimental results for storm-water column height values against inlet flow in litres per second. The numerical model results were compared to the experimental results at inflow rates of 45 l/s, 60 l/s, 90 l/s, 100 l/s, and 130 l/s. The curve output for the numerical (this study) and experimental results are shown in Fig. 9. The red graph represents the experimental storm-water column values while the blue graph represents the numerical storm-water column values. It is observed in Fig. 9, that there is a good agreement between the experimental results and the numerical results of this study.

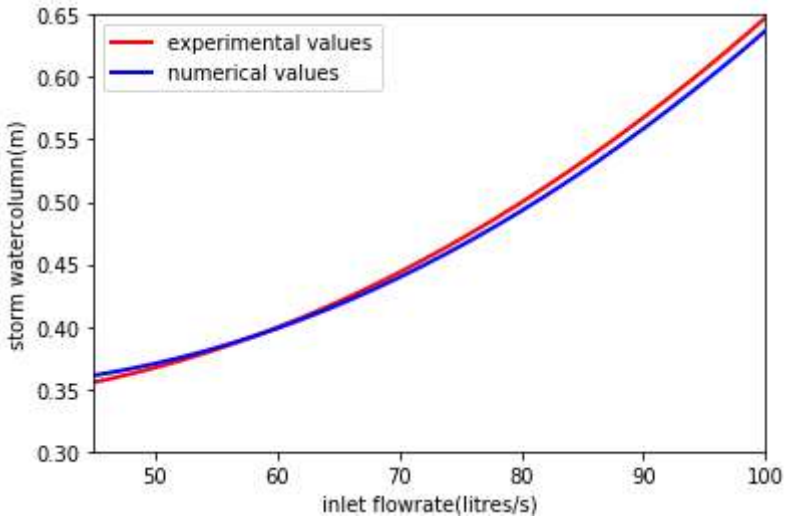

Figure 9: Comparison between numerical results of this study and experimental results

Experimental results show a free surface flow at storm-water column less than 0.4 m, and a pressurized flow at storm-water column greater than or equal to 0.4 m. The numerical values of this study agree with experimental values at surface flow and pressurized flow, Table 2. Figure 10 represents the surface flow of the numerical model of this study on manhole pipes at a storm-water column height value of 0.31 m, Fig. 11 represents the pressurized flow on manhole pipes for the numerical model of this study at storm-water column height value of 0.44 m

Table 2: Experimental vs numerical values on surface and pressurized flow

	Experimental (m)	Numerical (m)	Difference (m)
Surface flow	0.3	0.31	0.01
Pressurized flow	0.431	0.44	0.009

Figure 10: Pipes surface flow

Figure 11: Pipes pressurized flow

4.4 Velocity field

The velocity vector of the sewer overflow in the surcharged manhole is shown in Fig. 12. As can be observed, the velocity vectors are linear at the region of the inlet and outlet pipe, with proper direction from left to right. This indicates that the sewer flow at that region passes directly from the inlet to the outlet in straight paths. The linear flow in this region is influenced by the sewer flow that comes directly from the inlet to the outlet pipe. At regions above the inlet and outlet pipes, the velocity vectors take different directions at different places due to the random rotational motion of sewer flow as the pressure column is developed.

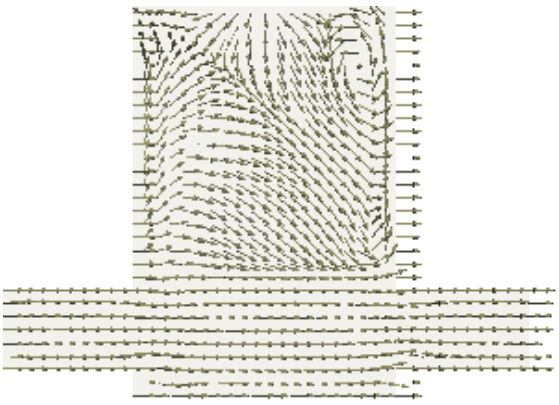

Figure 12: Flow direction

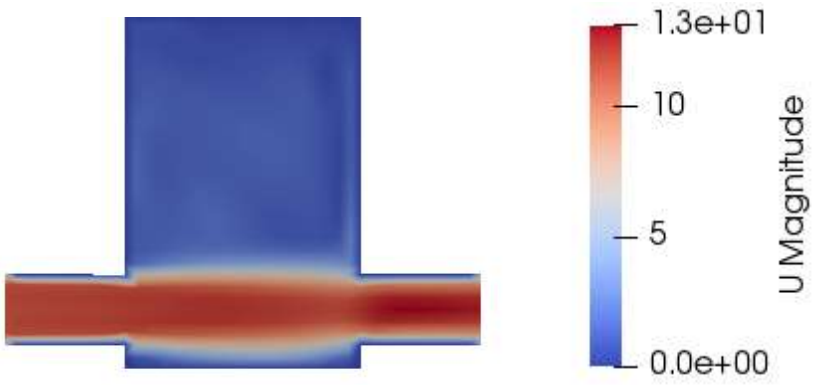

Figure 13: Velocity magnitude

The distribution of velocity magnitude is shown in Fig. 13. The velocity magnitude is higher at the horizontal region that lies inside the inlet and outlet pipe. The velocity takes its maximum magnitude value in this region due to the direct path of the sewer flow from the inlet to the outlet pipe. At the walls of the pipe, the velocity magnitude decreases compared to the centre of the pipes. This is due to the developed velocity profile of viscous flow on stationary walls. At regions inside the pressure head column, the sewer flow takes different values due to the random motion of the flow as it can be seen by different velocity colour distribution.

4.5 Pressure field

The pressure distribution of the overflowing storm-water in the manhole is shown in Fig. 14. Pressure values at the bottom of the manhole increase with increasing pressure head column in the manhole. However, the highest values of pressure are obtained at the bottom, opposite to the inlet pipe. This is because of the storm-water that hit directly the opposite walls from the inlet pipe. Higher pressure values are also found at edges which are the intersection between vertical walls of the manhole and the outlet pipe walls. At these edges, the stream of storm-water makes a direct hit as they find their way to the outlet pipe. Pressure distribution given in Fig. 14 is static pressure which decreases as the velocity of fluid increases. At the outlet pipe, the escaping velocity is higher than the inlet velocity. Therefore, the indicated static pressure at the outlet pipe decreases while dynamic pressure increase

The pressure head in the manhole develops through the random movement of storm-water currents. The backflow of storm-water after hitting the right walls exert some pressure at the bottom of the left wall. Figure 15 shows the pressure distribution at the bottom of the manhole, which indicates the highest values at the walls opposite to the inlet pipe, and considerably larger

values at the left wall due to backflow. The minimum pressure values are attained at the bottom centre.

Figure 14: Pressure distribution on the manhole

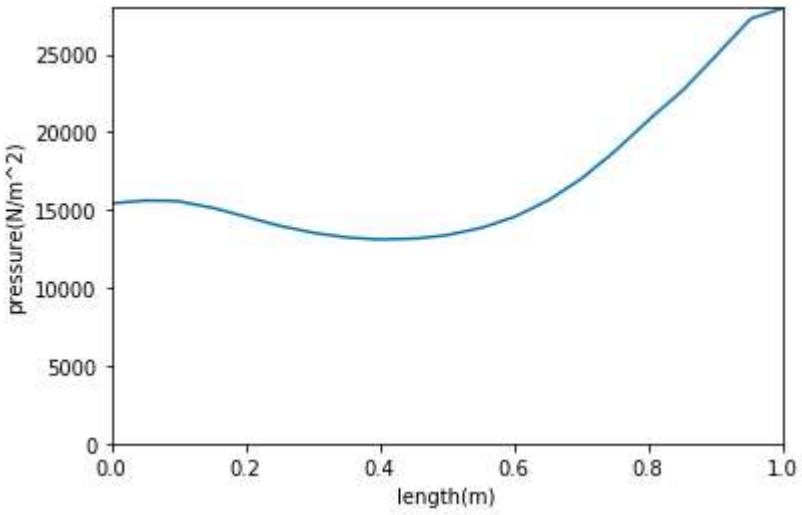

Figure 15: The pressure at the bottom

4.6 Uplifting forces

In this study, the storm-water overflow behaviour at the manhole is analysed numerically. The computation of pressure distribution and the force distribution acting on the manhole cover were carried out using filters from the OpenFOAM visualization tool, paraview 5.4.0. The bottom surface of the manhole cover was extracted independently, for the pressure and force distribution of storm-water, as it is the surface on the cover that faces the interaction with the hitting storm-water.

The forces acting on the manhole cover are due to the hitting of storm-water on the bottom wall of the cover as its pressure head is rising inside. The rising storm-water column inside the manhole consists of swirling storm currents. Due to the swirling of the storm-water currents, the storm-water hits the cover with different pressure values. Some areas of the cover receive higher values of pressure, causing high-intensity overflow in those directions. As can be inferred from Fig. 16, the results show those cover areas opposite to the outlet pipe experience the high intense storm overflow.

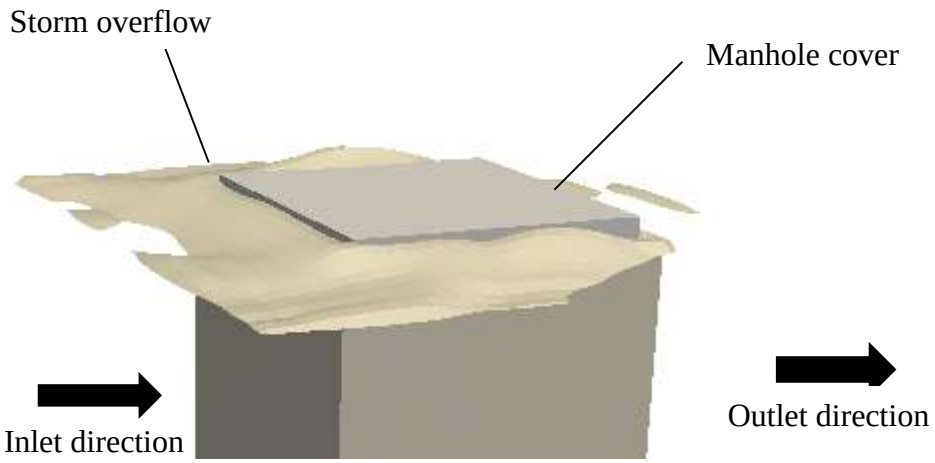

Figure 16: The direction of the intense overflow

This implies that the pressure exerted at the cover is not uniform, and it depends on the velocity direction upon hitting the wall. Figure 17 shows the non-uniform pressure distribution exerted by overflowing storm-water on the manhole cover at the 100^{th} second. The pressure values at this time lie between 78 N/m^2 and 1600 N/m^2. Areas of the cover that face the perpendicular velocity hit with storm-water receive the maximum value of hitting pressure, whereas areas of the cover that storm-water velocity direction is away from it, experience the minimum value of the hitting pressure.

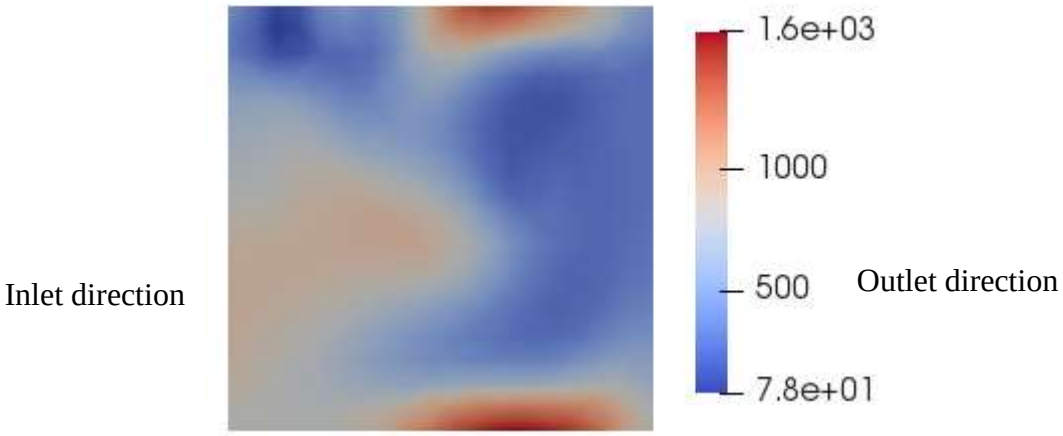

Figure 17: Non-uniform pressure distribution on a manhole cover

Observed in this study is that different pressure distributions acting on the manhole cover result in different force distributions as well. The pressure distribution was then averaged to determine the global pressure (global force) which is, the effective uplifting force that pushes the cover outward. The results of global pressure from the beginning of the simulation are given in Fig. 18.

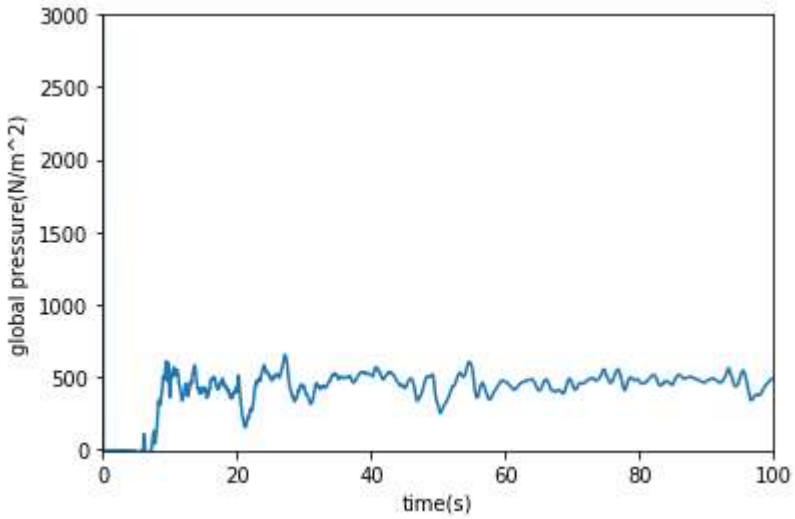

Figure 18: Storm-water global pressure on the manhole cover

It is observed that due to the fluctuation of the pressure field on manhole cover with time, the global pressure also fluctuates with time. The global pressure at the manhole cover starts at zero value and then increases in value, Fig. 18. After the storm-water starts overflowing, the global pressure acting on the manhole cover fluctuates about a constant mean. The average pressure acting on the manhole cover at each second was calculated by the OpenFOAM

visualization tool, paraview 5.4.0. The global pressure exerted on the manhole cover at the running time was taken as the average of all pressure acting on the cover at different particular times. The obtained constant mean global pressure acting on the manhole cover at the running time is 415.17 N/m^2. The cross-section area of the manhole cover is 1 m^2. Therefore, the global force variation with time is the same as the global pressure variation, as can be inferred from Fig. 19. At the overflow, the mean constant uplifting force of the storm-water is 415.17 N.

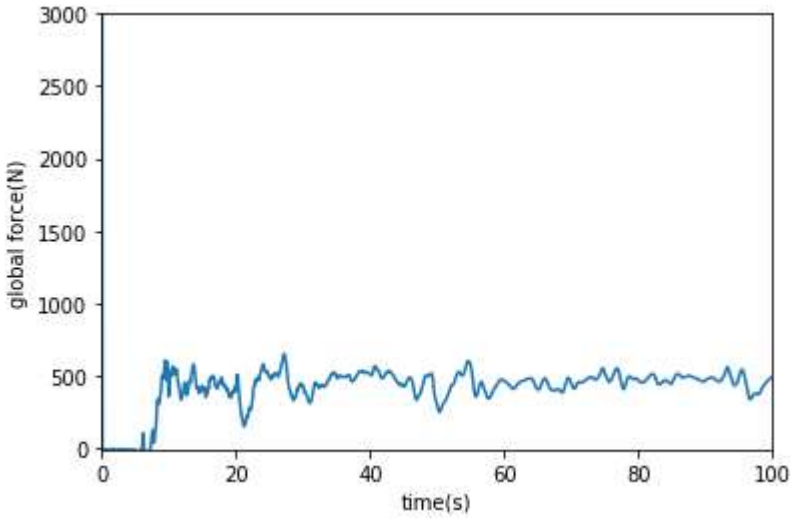

Figure 19: Storm-water uplifting forces

4.7 Comparison between inlet and outlet pipe diameter variations and manhole width (diameter) variations

An investigation was made on the extent of storm-water column rise inside the manhole. The rising-rate was compared between the variations of inlet and outlet pipe diameters and the variations of manhole width to determine which parameter supports much the rise of the storm-water column in the manhole. The interval of 0.025 m of pipe diameters was used to study the rate of wastewater rise in the manhole. Starting from 0.25 m, other pipe diameters that were used were 0.275 m, 0.3 m, 0.325 m, 0.35 m, 0.375 m, 0.4 m, 0.425 m, 0.45 m. In investigating the change in column height with change in manhole diameter, the diameter of the manhole was changed to an interval of 0.1 m. Different values used were 0.7 m, 0.8 m, 0.9 m, 1.0 m, 1.1 m, 1.2 m, 1.3 m, 1.4 m and 1.5 m. Figures 20 and 21 show the pipe diameter variations and manhole diameter variations against the storm-water column in manhole respectively.

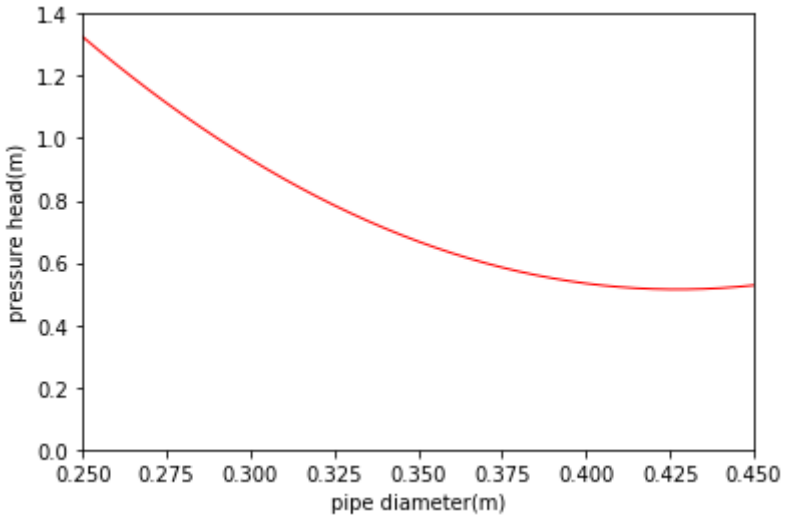

Figure 20: Pipe diameter variation with storm-water column

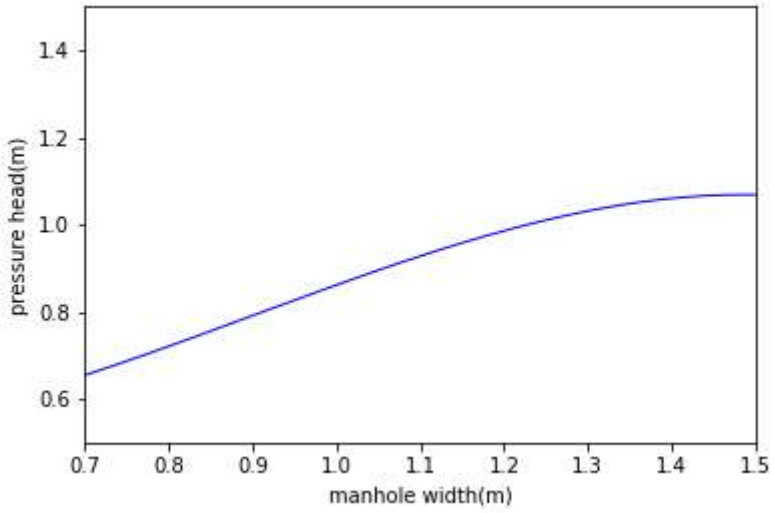

Figure 21: Manhole width variation with storm-water column

Figure 20 shows that at a constant inlet flow rate and manhole width, the storm-water column in the manhole decreases with increasing inlet and outlet pipe diameters connected to the manhole. That is, the larger the inlet and outlet pipe diameters are used on the manhole, the less is the rate of increase of storm-water column in the manhole. The smaller the pipe diameters are used in the manhole, the larger is the rate of increase storm-water column in the manhole.

Figure 21 is the graph of manhole width variation; it shows that at constant inlet and outlet pipe diameters and inlet flow rate, the variations of manhole width are proportional to changes of storm-water column height. The use of larger manhole width corresponds to the larger rate of rising of the storm-water column in the manhole. This is due to the fact that the increase of

manhole diameter increases the volume of storm-water to be reserved inside the manhole. With constant outlet pipe diameter, the discharge rate becomes small compared to the increased amount of storm-water kept in the manhole, making the storm-water column to increase rapidly.

Figure 22 shows the decrease of storm-water column height with the increase in manhole diameter when pipe diameters are increased. The use of large pipe diameters on large manholes increases the discharge rate of storm-water from the manhole. To reduce the rate of storm-water rise inside the manhole, larger manholes should never be used with smaller pipe diameters, as this tends to facilitate the overflow through the increased rate of the storm-water column. At manhole width of 0.9 m, there is a maximum storm-water pressure column which decreases for manhole width greater than 0.9 m. This shows that the use of larger pipes on manholes is significant on reducing the rate of storm-water column rise when manhole width is greater than 0.9 m.

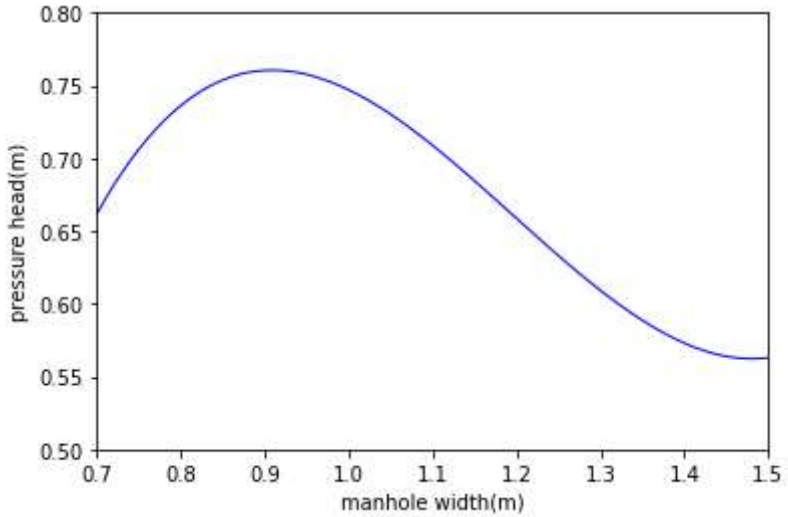

Figure 22: Manhole width variations with larger pipes

A comparison between Fig. 20 and Fig. 22 shows that; storm-water column reaches a larger maximum height in Fig. 20 than the maximum height value attained in Fig. 22. This shows that on manholes with larger width (or diameters), the use of larger inlet and outlet pipes is a better way to reduce the rate of storm-water column rise inside the manhole.

CHAPTER FIVE

CONCLUSION AND RECOMMENDATIONS

5.1 Conclusion

CFD has produced a realistic situation of manhole overflow as it occurs in a real-life situation. In modelling turbulence, the standard turbulence model, $k-\in$ model, and the volume of the fluid model, a model for phases modelling, together provide a proper prediction of turbulence flow in storm-water flow in sewer systems. The full Navier-Stokes equations are useful in giving a numerical representation of fluid flow related problems.

The general pressure at the bottom of the manhole increases as the storm-water column inside the manhole, increases. For the overflowed manhole, the highest pressure values are found at the edge which is the intersection between manhole walls and the outlet pipe walls and nearby regions of those edges. Velocity magnitude attains its highest values at the horizontal region that lies between the manhole and the inlet and outlet pipes. This is because in this region there is a direct influence of the flow from the inlet pipe to the outlet pipe.

At overflow, there is a different intensity overflow from the manhole. This is because of non-uniform pressure values exerted at manhole cover by the hitting storm-water column inside the manhole. Areas below the manhole cover that are opposite to the outlet pipe give the highest overflow intensity compared to other areas. The global uplifting forces of the rising storm-water column to the manhole cover increase in value until overflow occurs when they remain fluctuating about a constant value. For rectangular manhole with a cross-section area of 1 m^2, the uplifting force at the overflow is 415.17 N.

The manhole width (diameter) and pipe diameters affect the rate of rising of the storm-water column inside the manhole. The use of larger manhole pipes decreases the rate of rising of the storm-water column in the manhole. For the manhole width, the use of manhole with larger width (diameters), increases the rate at which storm-water column rises. However larger manholes with larger pipes decrease much the rate of column rise than the use of larger pipes only. Manhole overflow can be reduced by reducing the rate of storm-water column rise in the manhole. This is achieved by the use of larger manholes with larger inlet and outlet pipes.

5.2 Recommendations

Due to the fact that manhole cover delays the overflow, storm uplifting forces must be determined for each manhole size to establish the minimum weight of the cover. Manhole cover weights should be greater than the uplifting forces for both rectangular and circular manholes in use.

To reduce the rate of rise of storm-water inside manhole, manholes of width greater than 0.9 m should be used with inlet and outlet pipes of larger diameters. Further studies on manhole overflow should consider the hydrodynamic behaviour of the total network so that the general output of the system on the particular area can be given. Also the effect of transported solid materials on sewer flow in sewer systems should be considered in further studies.

REFERENCE

Bayon, A., Valero, D., García-bartual, R., & Jos, F. (2016). *Environmental Modelling & Software Performance assessment of OpenFOAM and FLOW-3D in the numerical modeling of a low Reynolds number hydraulic jump Vall e*. *80*, 322–335. https://doi.org/10.1016/j.envsoft.2016.02.018

Beg, M. N. A., Carvalho, R., Lopes, P., Leandro, J., & Melo, N. (2016). Numerical Investigation of the Flow Field inside a Manhole-Pipe Drainage System. *Hydraulic Structures and Water System Management. 6th IAHR International Symposium on Hydraulic Structures, 3706281608*, 1–11. https://doi.org/10.15142/T370628160853

Beg, N A, Carvalho, R. F., Leandro, J., Lopes, P., & Cartaxo, L. (2016). *Investigation of the Flow Field inside a Drainage System : Gully - PipeManhole*.https://doi.org/10.15142/T3859Z

Beg, Nazmul Azim, Carvalho, R. F., & Leandro, J. (2018). *E ff ect of surcharge on gully-manhole fl ow*. *19*, 224–236. https://doi.org/10.1016/j.jher.2017.08.003

Chang, T., Wang, C., Chen, A. S., & Djordjević, S. (2018). The influence of inlet drainage in modelling flow interactions between storm sewer system and overland surface. *Journal of Hydrology*, *559*, 541–555. https://doi.org/10.1016/j.jhydrol.2018.01.066

Date, A. W. (2017). *Computational Fluid Dynamics* (Issue October 2008). https://doi.org/10.1002/0471238961.compdate.a01

Duque, N., Duque, D., & Saldarriaga, J. (2017). Dynamic Programming over a Graph Modeling Framework for the Optimal Design of Pipe Series in Sewer Systems. *Procedia Engineering*, *186*, 61–68. https://doi.org/10.1016/j.proeng.2017.03.208

Factor, C., Pressure, I., Menon, E. S., & Manual, S. (2015). *Thermal Hydraulics Single-phase and Multiphase Flow in Natural Gas Production Systems*. https://www.sciencedirect.com/topics/engineering/isothermal-flow

Jo, J. B., Kim, J. S., & Yoon, S. E. (2018). Experimental estimation of the head loss coefficient at surcharged four-way junction manholes. *Urban Water Journal*, 1–10.https://doi.org/10.1080/1573062X.2018.1547408

Khare, P. (2015). Incompressible Flow. *ContemporaryPhysics*, *57*(1), 117–118. https://doi.org/10.1080/00107514.2015.1048302

Manholes, J. (2018). *Head Loss Reduction in Surcharged Four-Way Junction Manholes*. 1–20. https://doi.org/10.3390/w10121741

Meister, M., & Rauch, W. (2016). Wastewater treatment modelling with smoothed particle hydrodynamics. *Environmental Modelling and Software*, *75*, 206–211. https://doi.org/10.1016/j.envsoft.2015.10.010

Moeini, R., & Afshar, M. H. (2017). Arc Based Ant Colony Optimization Algorithm for optimal design of gravitational sewer networks. *Ain Shams Engineering Journal*, *8*(2), 207–223. https://doi.org/10.1016/j.asej.2016.03.003

Moukalled, F., Mangani, L., & Darwish, M. (2016). Implementation of boundary conditions in the finite-volume pressure-based method—Part I: Segregated solvers. *Numerical Heat Transfer, Part B: Fundamentals*, *69*(6), 534–562. https://doi.org/10.1080/10407790.2016.1138748

Nawrot, T., Matz, R., Błazejewski, R., & Spychala, M. (2018). A case study of a small diameter gravity sewerage system in Zolkiewka Commune, Poland. *Water (Switzerland)*, *10*(10). https://doi.org/10.3390/w10101358

Pastore, M. C. (2015). Reworking the relation between sanitation and the city in Dar es Salaam, Tanzania. *Environment and Urbanization*, *27*(2), 473–488. https://doi.org/10.1177/0956247815592285

Ramakrishna, M. (2011). Elements of computational fluid dynamics. *IIT Madras*. *2*.https://doi.org/10.1016/S0376-0421(00)00005-1

Ravelli, S., Barigozzi, G., Pasqua, F., Pieri, R., & Ponzini, R. (2014). *Numerical and experimental study for the prediction of the steady, three dimensional flow in a turbine nozzle vane cascade using OpenFOAM*. .https://www.semanticscholar.org/paper/Numerical-and-experimental-study-for-the-prediction-Ravelli-Barigozzi/10e9dec5c64df2be5686ce585df67324aa8ea19

Rocco, G., Coppola, G., & De Luca, L. (2010). The VOF method applied to the numerical simulation of a 2D liquid jet under gravity. *WIT Transactions on Engineering Sciences*, *69*, 207–217. https://doi.org/10.2495/AFM100181

Salih, A. (2011). *Conservation Equations of Fluid Dynamics*. *February*, 1–8. https://www.iist.ac.in/sites/default/files/people/fmeqns.pdf

Sánchez, F., Kaiser, A. S., Viedma, A., & Gómez, A. (2016). *Effects of the aeration on the fluid dynamic behaviour of a multi-zone activated sludge system*. *202*. https://doi.org/10.2495/WM160281

Sert, C. (2012). Chapter 1 Governing Equations of Fluid Flow and Heat Transfer. *Finite Element Analysis in Thermofluids*, 1–13. http://users.metu.edu.tr/csert/me582/ME582 Ch 01.pdf

Swamee, P. K., & Sharma, A. K. (2013). Optimal design of a sewer line using Linear Programming. *Applied Mathematical Modelling*, *37*(6), 4430–4439. https://doi.org/10.1016/j.apm.2012.09.041

Uddin, I., & Karim, M. (2017). Application of Volume Of Fluid (VOF) Method for Prediction of Wave Generated by Flow around Cambered Hydrofoil. *Procedia Engineering*, *194*, 82–89. https://doi.org/10.1016/j.proeng.2017.08.120

Villiers, N. De, Rooyen, G. C. Van, & Middendorf, M. (2019). *Sewer network design : Heuristic algorithm for hydraulic optimisation*. *59*(3), 48–56. https://doi.org/10.17159/2309-8775/2017/v59n3a6

Wang, J., Engineering, J., & Vasconcelos, J. G. (2019). *Investigation of manhole cover displacement during rapid filling of stormwater systems*. https://www.researchgate.net/publication/336197261_Investigation_of_manhole_cover_displacement_during_rapid_filling_of_stormwater_systems

Xue, S. C., & Barton, G. W. (2015). Incompressible fluid flow simulations with flow rate as the sole information at synthetic inflow and outflow boundaries. *International Journal for Numerical Methods in Fluids*, *78*(12), 739–760. https://doi.org/10.1002/fld.4039

Zhang, Z., & Chian, S. C. (2019). Importance of sidewall friction on manhole uplift during soil liquefaction. *Soil Dynamics and Earthquake Engineering*, *119*(August 2018), 51–61. https://doi.org/10.1016/j.soildyn.2018.12.028

APPENDICES

Appendix 1: snappyHexmeshDict

```
/*--------------------------------*- C++ -*----------------------------------*\
| =========                 |                                                 |
| \\      /  F ield         | OpenFOAM: The Open Source CFD Toolbox
|  \\    /   O peration     | Version:  5
|   \\  /    A nd           | Web:      www.OpenFOAM.org
|    \\/     M anipulation  |
\*---------------------------------------------------------------------------*/
FoamFile
{
    version     2.0;
    format      ascii;
    class       dictionary;
    object      snappyHexMeshDict;
}
// * * * * * * * * * * * * * * * * * * * * * * * * * * * * * * * * * * * * //

// Which of the steps to run
castellatedMesh true;
snap            true;
addLayers      false;


// Geometry. Definition of all surfaces. All surfaces are of class
// searchableSurface.
// Surfaces are used
// - to specify refinement for any mesh cell intersecting it
// - to specify refinement for any mesh cell inside/outside/near
// - to 'snap' the mesh boundary to the surface
geometry
{
    pipa
    {
        type triSurfaceMesh;
        file "pipa.stl";
    }
    inlet
    {
        type triSurfaceMesh;
        file "inlet.stl";
    }
    outlet
    {
        type triSurfaceMesh;
        file "outlet.stl";
    }
    outlets
    {
```

```
        type triSurfaceMesh;
        file "outlets.stl";
    }
    atmosphere
    {
        type triSurfaceMesh;
        file "atmosphere.stl";
    }
    belowcover
    {
        type triSurfaceMesh;
        file "belowcover.stl";
    }
    remaincover
    {
        type triSurfaceMesh;
        file "remaincover.stl";
    }
    layerWalls
    {
        type triSurfaceMesh;
        file "layerWalls.stl";
    }
    stationaryWalls
    {
        type triSurfaceMesh;
        file "stationaryWalls.stl";
    }
    refinementBox
    {
        type searchableBox;
        min (-1  1.48 -1);
        max (2   1.53 2);
    }
};
// Settings for the castellatedMesh generation.
castellatedMeshControls
{

    // Refinement parameters
    // ~~~~~~~~~~~~~~~~~~~~~

    // If local number of cells is >= maxLocalCells on any processor
    // switches from from refinement followed by balancing
    // (current method) to (weighted) balancing before refinement.
    maxLocalCells 1000000;

    // Overall cell limit (approximately). Refinement will stop immediately
    // upon reaching this number so a refinement level might not complete.
    // Note that this is the number of cells before removing the part which
    // is not 'visible' from the keepPoint. The final number of cells might
```

```
// actually be a lot less.
maxGlobalCells 20000000;

// The surface refinement loop might spend lots of iterations refining just a
// few cells. This setting will cause refinement to stop if <= minimumRefine
// are selected for refinement. Note: it will at least do one iteration
// (unless the number of cells to refine is 0)
minRefinementCells 0;

// Number of buffer layers between different levels.
// 1 means normal 2:1 refinement restriction, larger means slower
// refinement.
nCellsBetweenLevels 3;

// Explicit feature edge refinement
// ~~~~~~~~~~~~~~~~~~~~~~~~~~~~~~~

// Specifies a level for any cell intersected by its edges.
// This is a featureEdgeMesh, read from constant/triSurface for now.
features
(
     {
         file "pipa.eMesh";
         level 1;
     }
     {
         file "inlet.eMesh";
         level 1;
     }
     {
         file "outlet.eMesh";
         level 1;
     }
     {
         file "outlets.eMesh";
         level 1;
     }
     {
         file "atmosphere.eMesh";
         level 1;
     }
     {
         file "belowcover.eMesh";
         level 1;
     }
     {
         file "remaincover.eMesh";
         level 1;
     }
     {
         file "layerWalls.eMesh";
```

```
        level 1;
    }
    {
        file "stationaryWalls.eMesh";
        level 1;
    }
);

// Surface based refinement
// ~~~~~~~~~~~~~~~~~~~~~~~~

// Specifies two levels for every surface. The first is the minimum level,
// every cell intersecting a surface gets refined up to the minimum level.
// The second level is the maximum level. Cells that 'see' multiple
// intersections where the intersections make an
// angle > resolveFeatureAngle get refined up to the maximum level.

refinementSurfaces
{
    inlet
    {
        // Surface-wise min and max refinement level
        level (1 1);
        patchInfo
      {
        type patch;
      }
    }
    outlet
    {
        // Surface-wise min and max refinement level
        level (1 1);
        patchInfo
      {
        type patch;
      }
    }
    outlets
    {
        // Surface-wise min and max refinement level
        level (1 1);
        patchInfo
      {
        type patch;
      }
    }
    atmosphere
    {
        // Surface-wise min and max refinement level
        level (1 1);
        patchInfo
```

```
        {
            type patch;
        }
    }
    belowcover
    {
        // Surface-wise min and max refinement level
        level (1 1);
        patchInfo
        {
            type wall;
        }
    }
    remaincover
    {
        // Surface-wise min and max refinement level
        level (1 1);
        patchInfo
        {
            type wall;
        }
    }
    layerWalls
    {
        // Surface-wise min and max refinement level
        level (1 1);
        patchInfo
        {
            type wall;
        }
    }
    stationaryWalls
    {
        // Surface-wise min and max refinement level
        level (1 1);
        patchInfo
        {
            type wall;
        }
    }
}

resolveFeatureAngle 45;


// Region-wise refinement
// ~~~~~~~~~~~~~~~~~~~~~~

// Specifies a refinement level for cells in relation to a surface. One of
// three modes
// - distance. 'levels' specifies per the distance to the surface the
```

```
    //   wanted refinement level. The distances need to be specified in
    //   descending order.
    // - inside. 'levels' is only one entry and only the level is used. All
    //   cells inside the surface get refined up to the level. The surface
    //   needs to be closed for this to be possible.
    // - outside. Same but cells outside.

    refinementRegions
    {
      pipa
      {
             mode inside;
       levels ((1 1));
      }
      refinementBox
      {
             mode inside;
       levels ((1 1));
      }
    }

    // Mesh selection
    // ~~~~~~~~~~~~~~

    // After refinement patches get added for all refinementSurfaces and
    // all cells intersecting the surfaces get put into these patches. The
    // section reachable from the locationInMesh is kept.
    // NOTE: This point should never be on a face, always inside a cell, even
    // after refinement.
    locationInMesh (0.5 1 0.5);


    // Whether any faceZones (as specified in the refinementSurfaces)
    // are only on the boundary of corresponding cellZones or also allow
    // free-standing zone faces. Not used if there are no faceZones.
    allowFreeStandingZoneFaces true;
}

// Settings for the snapping.
snapControls
{
    //- Number of patch smoothing iterations before finding correspondence
    //  to surface
    nSmoothPatch 3;

    //- Relative distance for points to be attracted by surface feature point
    //  or edge. True distance is this factor times local
    //  maximum edge length.
    //    tolerance 4.0;
    tolerance 1.0;
```

```
    //- Number of mesh displacement relaxation iterations.
    nSolveIter 300;

    //- Maximum number of snapping relaxation iterations. Should stop
    //  before upon reaching a correct mesh.
    nRelaxIter 5;

    nFeatureSnapIter 10;
}

// Settings for the layer addition.
addLayersControls
{
    // Are the thickness parameters below relative to the undistorted
    // size of the refined cell outside layer (true) or absolute sizes (false).
    relativeSizes true;

    // Per final patch (so not geometry!) the layer information
    layers
    {
        stationaryWalls1
        {
            nSurfaceLayers 5;
        }
        stationaryWalls2
        {
            nSurfaceLayers 5;
        }
        stationaryWalls3
        {
            nSurfaceLayers 5;
        }
    }

    // Expansion factor for layer mesh
    expansionRatio 1.5;


    // Wanted thickness of final added cell layer. If multiple layers
    // is the thickness of the layer furthest away from the wall.
    // Relative to the undistorted size of the cell outside layer.
    // See relativeSizes parameter.
    finalLayerThickness 0.7;

    // Minimum thickness of cell layer. If for any reason layer
    // cannot be above minThickness do not add a layer.
    // See relativeSizes parameter.
    minThickness 0.25;

    // If points get not extruded do nGrow layers of connected faces that are
    // also not grown. This helps convergence of the layer addition process
```

```
    // close to features.
    // Note: changed(corrected) w.r.t 17x! (didn't do anything in 17x)
    nGrow 0;

    // Advanced settings

    // When not to extrude surface. 0 is a flat surface, 90 is when two faces
    // are perpendicular
    featureAngle 60;

    // Maximum number of snapping relaxation iterations. Should stop
    // before upon reaching a correct mesh.
    nRelaxIter 5;

    // Number of smoothing iterations of surface normals
    nSmoothSurfaceNormals 1;

    // Number of smoothing iterations of interior mesh movement direction
    nSmoothNormals 3;

    // Smooth layer thickness over surface patches
    nSmoothThickness 10;

    // Stop layer growth on highly warped cells
    maxFaceThicknessRatio 0.5;

    // Reduce layer growth where ratio thickness to medial
    // distance is large
    maxThicknessToMedialRatio 0.3;

    // Angle used to pick up medial axis points
    // Note: changed(corrected) w.r.t 17x! 90 degrees corresponds to 130 in 17x.
    minMedianAxisAngle 90;

    // Create buffer region for new layer terminations
    nBufferCellsNoExtrude 0;


    // Overall max number of layer addition iterations. The mesher will exit
    // if it reaches this number of iterations; possibly with an illegal
    // mesh.
    nLayerIter 50;

    // Max number of iterations after which relaxed meshQuality controls
    // get used. Up to nRelaxIter it uses the settings in meshQualityControls,
    // after nRelaxIter it uses the values in meshQualityControls::relaxed.
    nRelaxedIter 20;
}
```

```
// Generic mesh quality settings. At any undoable phase, these determine
// where to undo.
meshQualityControls
{
    #include "meshQualityDict"
}

// Advanced

// Flags for optional output
// 0 : only write final meshes
// 1 : write intermediate meshes
// 2 : write volScalarField with cellLevel for postprocessing
// 4 : write current intersections as .obj files
debug 0;

// Merge tolerance. Is a fraction of the overall bounding box of the initial mesh.
// Note: the write tolerance needs to be higher than this.
mergeTolerance 1E-6;


// ************************************************************************* //
```